A&A 529, A74 (2011)
DOI: 10.1051/0004-6361/201016121

Astronomy & Astrophysics

Laboratory H_2O:CO_2 ice desorption data: entrapment dependencies and its parameterization with an extended three-phase model

E. C. Fayolle[1], K. I. Öberg[2], H. M. Cuppen[1,3], R. Visser[3], and H. Linnartz[1]

[1] Sackler Laboratory for Astrophysics, Leiden Observatory, Leiden University, PO Box 9513, 2300 RA Leiden, The Netherlands
e-mail: fayolle@strw.leidenuniv.nl
[2] Harvard-Smithsonian Center for Astrophysics, MS 42, 60 Garden Street, Cambridge, MA 02138, USA
[3] Leiden Observatory, Leiden University, PO Box 9513, 2300 RA Leiden, The Netherlands

Received 10 November 2010 / Accepted 21 February 2011

ABSTRACT

Context. Ice desorption affects the evolution of the gas-phase chemistry during the protostellar stage, and also determines the chemical composition of comets forming in circumstellar disks. From observations, most volatile species are found in H_2O-dominated ices.
Aims. The aim of this study is first to experimentally determine how entrapment of volatiles in H_2O ice depends on ice thickness, mixture ratio and heating rate, and second, to introduce an extended three-phase model (gas, ice surface and ice mantle) to describe ice mixture desorption with a minimum number of free parameters.
Methods. Thermal H_2O:CO_2 ice desorption is investigated in temperature programmed desorption experiments of thin (10–40 ML) ice mixtures under ultra-high vacuum conditions. Desorption is simultaneously monitored by mass spectrometry and reflection-absorption infrared spectroscopy. The H_2O:CO_2 experiments are complemented with selected H_2O:CO, and H_2O:CO_2:CO experiments. The results are modeled with rate equations that connect the gas, ice surface and ice mantle phases through surface desorption and mantle-surface diffusion.
Results. The fraction of trapped CO_2 increases with ice thickness (10–32 ML) and H_2O:CO_2 mixing ratio (5:1–10:1), but not with one order of magnitude different heating rates. The fraction of trapped CO_2 is 44–84% with respect to the initial CO_2 content for the investigated experimental conditions. This is reproduced quantitatively by the extended three-phase model that is introduced here. The H_2O:CO and H_2O:CO_2:CO experiments are consistent with the H_2O:CO_2 desorption trends, suggesting that the model can be used for other ice species found in the interstellar medium to significantly improve the parameterization of ice desorption.

Key words. astrochemistry – methods: laboratory – methods: analytical – ISM: molecules

1. Introduction

In pre-stellar cores, cold outer protostellar envelopes and protoplanetary disk midplanes, most molecules, except for H_2, are frozen out on dust grains, forming ice mantles. The main ice component in most lines of sight is H_2O, followed by CO and CO_2, with a typical abundance of $(0.5-1.5) \times 10^{-4}$ for H_2O ice with respect to H_2 around solar-type protostars (van Dishoeck 2006). Infrared observations of pre-stellar cores show that most CO_2 ice and some of the CO ice is mixed with H_2O (Knez et al. 2005). The remaining CO and CO_2 are found in separate ice layers. Based on these observations, H_2O and CO_2 are thought to form simultaneously on the grain surface during the early stage of cloud formation. When the cloud becomes denser, gas phase CO freezes out on top of the water-rich ice, resulting in a bi-layered ice mantle, as described in Pontoppidan et al. (2008).

Once the pre-stellar core starts collapsing into a protostar, it heats its environment, including the icy grains. This results in the desorption of the CO-rich layer into the gas phase, in structural changes in the water-rich ice layer, and eventually in the desorption of the water-rich layer (Pontoppidan et al. 2008). Such an ice desorption scheme provides most of the gas phase reactants for the chemistry taking place at later stages in these warm regions (Doty et al. 2004). It is therefore crucial to understand ice mixture desorption and to effectively implement it in astrochemical networks. The aim of this study is to provide a laboratory basis for this process and to demonstrate how it can be modeled both in the laboratory and in space.

Laboratory experiments have provided most of the current knowledge about ice thermal desorption, including desorption energies for most pure simple ices (Sandford & Allamandola 1988, 1990; Fraser et al. 2001; Collings et al. 2004; Öberg et al. 2005; Brown & Bolina 2007; Burke & Brown 2010). Desorption from ice mixtures differs from pure ice desorption because of different binding energies between the mixture components (e.g., the CO binding energy increases from 830 K in pure ice to 1180 K in H_2O-dominated ice mixtures Collings et al. 2003) and because of trapping of volatile species in the H_2O hydrogen-bonding ices (Collings et al. 2004). Volatile components therefore desorb from H_2O-rich ice mixtures at a minimum of two different temperatures, corresponding to the desorption of the species from the surface of the H_2O ice and from molecules trapped inside the bulk of the H_2O ice, which only start desorbing at the onset of H_2O desorption. Additional desorption is sometimes observed at the temperature for pure volatile ice desorption and during ice re-structuring, e.g., at the H_2O phase

change from amorphous to crystalline (Viti et al. 2004). This H_2O restructuring occurs at ~140 K in the laboratory (for astrophysical timescales the re-structuring temperature and desorption temperature decrease), which is close to the onset of H_2O desorption (Collings et al. 2004).

Of the different ice mixture desorption features, the entrapment of volatile species in H_2O ice is astrochemically the most important to quantify. The trapping of CO in a water ice results in a factor of five increase in the effective desorption temperature. In a recent cloud core collapse model, this corresponds to trapped CO desorbing at 30 AU from the protostar compared to pure CO ice desorbing at 3000 AU. The case is less dramatic, but still significant, for CO_2, which desorbs at ~300 AU when pure, and at 30 AU if trapped in H_2O ice (Aikawa et al. 2008; Visser et al. 2009). Efficient ice trapping may therefore allow some volatiles to stay frozen on the dust grains during accretion of envelope material onto the forming protoplanetary disk (Visser et al. 2009).

There are only a few models that have incorporated the effects of ice mixture desorption. Collings et al. (2004) investigated the desorption of 16 astrophysically relevant species from H_2O:X 20:1 ice mixtures. Viti et al. (2004) and Visser et al. (2009) used the results of Collings et al. (2004) to split up the abundance of volatiles in up to four different flavors, with different desorption temperatures. These correspond to the fraction of each ice desorbing at the pure ice desorption temperature, from a H_2O surface, during H_2O ice restructuring and with H_2O, respectively. This approach has provided information on the potential importance of ice trapping for the chemical evolution during star formation. However, this model does not take into account specific ice characteristics such as ice thickness, volatile concentration and heating rate, on which the amount of trapped volatiles in the water ice may also depend (Sandford & Allamandola 1988). These characteristics need to be determined experimentally to correctly parameterize step models, where such are sufficient to model ice desorption. Strong dependencies on e.g. ice thickness or concentration would however warrant the development of a more continuous parameterization of ice desorption than the assignment of flavors.

These dependencies are naturally included in a few ice mixture desorption models of specific binary ices (Collings et al. 2003; Bisschop et al. 2006). The molecular specificity of these models, together with a large number of fitting parameters has, however, prevented their incorporation into larger astrochemical models. Therefore, in most gas-grain networks, desorption is still treated as if ices were pure, disregarding volatile entrapment in the water matrix (e.g. Aikawa et al. 2008).

Another problem with current gas-grain codes is that evaporation is often incorporated as a first-order process, while it is experimentally found to be a zeroth-order process with respect to the total ice abundance for ices thicker than one monolayer. Desorption models from the last decades have shown the necessity of using a zeroth order kinetics (Fraser et al. 2001; Collings et al. 2003). Incorporating ice desorption as a first-order process with respect to the total ice abundance effectively means that molecules throughout the whole ice are allowed to desorb at the same time, which is non-physical (Fraser et al. 2001; Bisschop et al. 2006). This can be solved by treating the bulk and surface of the ice as separate phases as it has been done by Pontoppidan et al. (2003) and Pontoppidan et al. (2008) for CO ice desorption and by Collings et al. (2005) for H_2O desorption and crystallization. Its successful use in astrochemical models makes this approach an attractive option to parameterize laboratory ice desorption, since the results can then be easily transferred into an astrophysical context. In this family of models, molecules are only allowed to desorb from the surface, which is continuously replenished by molecules coming from the mantle, and therefore the desorption kinetics are automatically treated correctly. This model results in a zeroth-order desorption behavior, in agreement with the experiments, since the number of molecules available for desorption remains constant in time. The model also results in trapping of volatiles in the bulk of the ice since the mantle molecules cannot desorb into the gas phase. The three-phase model we build on was first introduced by Hasegawa & Herbst (1993), but despite its advantages in treating different ice processes, it has not been generally used for ice mixture desorption, nor has it been further developed, presumably because it did not correctly reproduce the experimentally observed amount of volatiles trapped in the water ice.

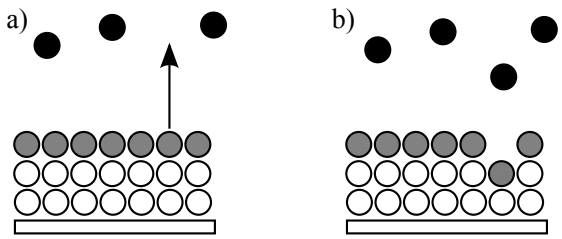

Fig. 1. Cartoon defining the ice mantle (white), ice surface (gray), and gas phase (black) according to the Hasegawa & Herbst (1993) three-phase model. Panels **a)** and **b)** show the different phases before and after a desorption event.

The goals of the present study are first to experimentally characterize how the trapping efficiency of CO_2 in H_2O ice depends on different ice characteristics (with complementary experiments on CO and tertiary mixtures) and second to use these experiments as a guide to improve our understanding of the trapping process within the three-phase model framework. The description of the extended three-phase model is explained in Sect. 2.1. The experiments used to get information on the volatile entrapment and to calibrate the model are described in Sect. 3. Laboratory results on H_2O:CO_2 ices, complemented by H_2O:CO and H_2O:CO_2:CO ice desorption results, are presented in Sect. 4. Section 5 presents the model fitting parameters and model results. Finally, the consequences of treating ice mixture desorption with the extended three-phase model under astrophysical conditions are discussed in Sect. 6.

2. Desorption model

This study addresses the desorption of volatiles mixed with water and how to predict the fractions of volatiles in the ice and gas phase during a warm-up of the ice. The model is a system of rate equations based on the Hasegawa & Herbst (1993) model, but with the addition of diffusion. It aims at providing a solution for the amount of volatiles trapped in water with respect to the ice characteristics that can be directly included into astrochemical models, as used by Viti et al. (2004) and Visser et al. (2009). The model applies to species in the water-rich ice layer; the interface with an upper CO-rich ice layer is not treated here.

2.1. Basic three-phase model

The model used here to predict the trapping of volatile species in a water dominated ice is based on the three-phase model by Hasegawa & Herbst (1993). In this model, gas-grain interactions are addressed by considering three phases: the gas phase,

the surface of the ice and the bulk/mantle of the ice (Fig. 1). The original model includes reactions between species in both gas and solid phase, as well as accretion from the gas to the ice and thermal and non-thermal desorption. Thermal desorption alone is presented here. The model is based on the principle that molecules can only desorb from the surface into the gas phase and that the mantle molecules can only migrate to the surface following the desorption of a surface molecule. The time-dependent gas abundance of species i is given by

$$\frac{\mathrm{d}n_i^{\mathrm{g}}}{\mathrm{d}t} = R_{\mathrm{evap}} \tag{1}$$

where,

$$R_{\mathrm{evap}} = \left(\nu\, \mathrm{e}^{-E_i/T}\right) n_i^{\mathrm{s}} \tag{2}$$

with n_i^{g} and n_i^{s} the gas phase and surface abundance of species i, respectively, E_i its binding energy in K, and ν a pre-exponential factor taken equal to 10^{12} s^{-1}, which is a standard value for physisorbed species (Biham et al. 2001). The surface abundance of species i can be written as:

$$\frac{\mathrm{d}n_i^{\mathrm{s}}}{\mathrm{d}t} = -R_{\mathrm{evap}} + R_{\mathrm{repl}} \tag{3}$$

where,

$$R_{\mathrm{repl}} = \alpha \left[\sum_j \left(\nu\, \mathrm{e}^{-E_j/T}\right) n_j^{\mathrm{s}}\right] \frac{n_i^{\mathrm{m}}}{\sum_j n_j^{\mathrm{m}}} \tag{4}$$

where n_i^{m} is the mantle abundance of species i, $\sum n_j^{\mathrm{m}}$ the total number of molecules in the mantle and α is the ice coverage on the surface, which is set to 2 ML to account for surface roughness. The first term in Eq. (3) represents the loss of molecules i from the surface by thermal desorption. The second term is related to the replenishment of the surface sites by mantle molecules: the empty sites created by the desorption of any type of species from the surface, $\sum_j (\nu\, \mathrm{e}^{-E_j/T}) n_j^{\mathrm{s}}$, are statistically filled by molecules coming from the mantle. The probability for these molecules to be species of type i is equal to its mantle fraction, $\frac{n_i^{\mathrm{m}}}{\sum n_j^{\mathrm{m}}}$. The mantle abundance, n_i^{m}, of species i changes according to

$$\frac{\mathrm{d}n_i^{\mathrm{m}}}{\mathrm{d}t} = -R_{\mathrm{repl}}. \tag{5}$$

Because of the term $\frac{n_i^{\mathrm{m}}}{\sum n_j^{\mathrm{m}}}$, the replenishment of the surface phase by the mantle molecules during ice mixture desorption depends only on the mixing ratio of each species in this model, e.g., for a H_2O:CO_2 1:1 ice mixture, a molecule that desorbs into the gas phase has a 50% chance to be replaced by a water molecule and a 50% chance to be replaced by a CO_2 molecule. This results in desorption of some volatile species around the pure ice desorption temperature and the rest remains trapped in the water ice since water molecules quickly saturate the surface phase.

The ice abundances n_i^{s} and n_i^{m} are all in cm^{-3}, a unit directly related to the gas phase abundance. The abundance of species i on the surface is defined via the relation

$$n_i^{\mathrm{s}} = N_i^{\mathrm{s}}\, n^{\mathrm{d}} \tag{6}$$

where N_i^{s} is the average number of molecules i on the grain surface, and n^{d} is the dust abundance. The same relation applies for the mantle abundance.

2.2. Extended three-phase model

The original three-phase model does not account for the preferred replenishment of the surface phase by volatile mantle species or that volatile species may diffuse more easily in the ice compared to water. Öberg et al. (2009b) showed that this diffusion can result in segregation of the ice components, which is important for temperatures well below the desorption energy of most volatile species in an ice mixture. This demixing mechanism changes the surface replenishment probabilities proposed in the original three-phase model by Hasegawa & Herbst (1993). Our proposed extension of the three-phase model accounts for this by introducing a mantle-surface diffusion term. Trapping of volatiles still occurs, but the surface-mantle diffusion of volatiles is enhanced compared to the original model, resulting in that more than 50% of the empty sites are filled by volatiles species. Quantitatively, this changes the surface and mantle abundances n_i^{s} and n_i^{m} as follows:

$$\frac{\mathrm{d}n_i^{\mathrm{s}}}{\mathrm{d}t} = -R_{\mathrm{evap}} + R_{\mathrm{repl}} + R_i^{\mathrm{diff}}, \tag{7}$$

and

$$\frac{\mathrm{d}n_i^{\mathrm{m}}}{\mathrm{d}t} = -R_{\mathrm{repl}} - R_i^{\mathrm{diff}} \tag{8}$$

with

$$R_i^{\mathrm{diff}} = f_i\, \nu \left[n_{\mathrm{H_2O}}^{\mathrm{s}} \frac{n_i^{\mathrm{m}}}{\sum_j n_j^{\mathrm{m}}}\, \mathrm{e}^{-E_{\mathrm{diff}}/T} - n_i^{\mathrm{s}} \frac{n_{\mathrm{H_2O}}^{\mathrm{m}}}{\sum_j n_j^{\mathrm{m}}}\, \mathrm{e}^{-E_{\mathrm{diff}}/T}\right], \tag{9}$$

and

$$E_{\mathrm{diff}} = \left(\epsilon_{\mathrm{H_2O}-i}^{\mathrm{swap}} - \frac{E_{\mathrm{H_2O}} - E_i}{2}\right) \tag{10}$$

for $i \neq \mathrm{H_2O}$, and where $\epsilon_{\mathrm{H_2O}-i}^{\mathrm{swap}}$ is the energy barrier for a volatile molecule i and a water molecule to swap (i.e. change position) within the ice and f_i a fraction between 0 and 1 that is described below. The expression for the gas phase abundance remains unchanged (see Eq. (1)). The diffusion term R_i^{diff} is added to the surface abundance (subtracted from the mantle abundance) to enhance the mantle to surface circulation for a volatile species i at the expense of the water, thus, R_i^{diff} is expressed differently for volatile and water molecules. The volatile ice diffusion rate depends on the balance of the probability of volatile molecules to move from the mantle to the surface at the expense of a water molecule and on the probability of the reverse process. This swapping process probability depends on the energy barrier $\epsilon_{\mathrm{H_2O}-i}^{\mathrm{swap}}$ of the process and on the energy difference before and after the swap, equal to $E_{\mathrm{H_2O}} - E_i$. The diffusion rate for the water molecules is the negative sum of the diffusion rates for the volatiles, $R_{\mathrm{H_2O}}^{\mathrm{diff}} = -\sum_i R_i^{\mathrm{diff}}$, since the total abundance of molecules in the mantle and in the surface is not affected by the diffusion process. A similar formalism was used to describe H_2O:CO_2 segregation in Öberg et al. (2009b); an exchange of a surface H_2O molecule and a mantle volatile is generally energetically favorable because H_2O forms stronger bonds than volatile species and a mantle H_2O molecule can form more bonds compared to a surface H_2O molecule.

From segregation studies of binary ices, it has become clear that only a limited fraction of the mantle participates in the mantle-surface circulation and that this fraction depends on the

initial ice mixture ratio (Öberg et al. 2009b). This is represented by the fraction f_i

$$f_i = 1 - \frac{n_i^{\mathrm{m,ini}} - c_i(x_i^{\mathrm{ini}})^\beta}{n_i^{\mathrm{m}}} \quad (11)$$

where $n_i^{\mathrm{m,ini}}$ is the number of mantle molecules i initially in the ice, c_i an empirical factor determined for each volatile i, and x_i^{ini} the initial mixing ratio of volatiles i with respect to water. The expression $c_i(x_i^{\mathrm{ini}})^\beta$ describes the number of mantle molecules available for segregation for a particular ice mixture before the onset of desorption and follows the form found by Öberg et al. (2009b) in ice segregation experiments when β is set equal to 2. The term $n_i^{\mathrm{m,ini}} - c_i(x_i^{\mathrm{ini}})^\beta$ is the number of mantle molecules protected from segregation. When the later expression exceeds the current number of volatile mantle molecules n_i^{m}, f_i reaches zero and segregation stops, i.e., the diffusion of volatile mantle molecules to the surface stops. Thus this definition results in a gradual slowdown of the "upward" mantle-surface diffusion of volatile species, regulating the trapping characteristics of H_2O ice for different volatiles.

We have tested the performance of this extended three-phase model on the desorption of mixed H_2O:CO_2 ices by comparing model and experimental TPD experiments, where the model TPDs are constructed using the rate Eqs. (1), (7) and (8). In the model TPDs the initial ice temperature is raised in steps proportional to the heating rate and at each time step the rate equations from the three-phase model are applied to calculate the temperature dependent desorption and diffusion rates. The desorption rate of the volatile is what is plotted in the TPD curves.

TPD experiments of pure ices are performed to determine the binding energies E_i. The other free parameters that are used to optimize the model are the swapping energies $\epsilon^{\mathrm{swap}}_{\mathrm{H_2O}-i}$ between H_2O molecules and volatiles i and the empirical factor c_i used to parameterize the diffusion of volatiles i from the mantle to the surface. These two parameters are determined by performing TPD experiments of binary ice mixtures of H_2O:CO_2 with different mixing ratios, thicknesses and heating rates and by comparing the output of the model with the experimental trends, i.e., the amount of volatile species that remains trapped in the water ice at temperatures higher than the desorption temperature of the volatile species.

It is important to note that the model does not include the finite pumping speed during experiments. This will affect the derived desorption barriers and these are therefore not meant to replace the ones derived from more detailed pure ice experiments in the literature. As long as the pumping rate is constant with temperature, excluding the pumping rate will not affect the determined ice fraction that desorbs at a low temperatures versus the fraction that desorbs with H_2O. This is a reasonable assumption above the pure volatile ice desorption temperatures, where cryopumping is no longer efficient. The derivation of c_i and $\epsilon^{\mathrm{swap}}_{\mathrm{H_2O}-i}$ should therefore not be affected by this simplification.

3. Experiments

3.1. Experimental parameters

The experiments in this study are chosen to simultaneously provide data directly relevant to ice desorption in different astrophysical environments (with different ices) and to construct a proof-of-concept model for ice mixture desorption. The focus is on CO_2 desorption from H_2O ice mixtures, one of the most important ice systems around protostars, with supporting experiments on CO desorption. While interstellar ices are expected to be complex mixtures, it is still useful to investigate desorption from binary H_2O:volatile ice mixtures since the H_2O:volatile interactions are expected to dominate the desorption process in space, both because H_2O is the major ice constituent and because H_2O generally forms stronger bonds with itself and with volatiles than volatiles do. This hypothesis has been further tested by performing TPD experiments of two tertiary H_2O:CO_2:CO ice mixtures.

The ice thickness and structure in the experiments are chosen to be as similar as possible to the existing observational constraints on interstellar ices. Interstellar ices are estimated to be less than 100 monolayers (ML) thick from the maximum amount of oxygen available for ice formation. The experimentally grown ices are between 10 and 40 ML, since it is only possible to quantify ice thicknesses up to a certain limit (40 ML in our case) using reflection-absorption infrared spectroscopy (Teolis et al. 2007). Information on ice structure in space is limited, but the lack of a water dangling vibration at 3700 cm^{-1} suggests a less porous ice than typically produced in the laboratory. We minimized the porosity of ice analogues by injecting gas perpendicularly to the cold surface when growing the ices (Stevenson et al. 1999; Kimmel et al. 2001).

3.2. Experimental procedures

All desorption experiments are performed with CRYOPAD. This set-up has been described in detail elsewhere (Fuchs et al. 2006). The set-up consists of an ultra high vacuum (UHV) chamber with a base pressure of $\sim 10^{-10}$ mbar at room temperature. Ices are grown on a gold-coated substrate situated at the center of the chamber that can be cooled down to 16 K by a close cycle He cryostat. The relative sample temperature is controlled with a precision of 0.1 K using a resistive heating element and a temperature control unit. The absolute sample temperature is given with a 2 K uncertainty. The system temperature is monitored with two thermocouples, one mounted on the substrate face, the other on the heater element.

A fourier transform spectrometer is used for reflection-absorption infrared spectroscopy (FT-RAIRS) to record vibrational absorption signatures of molecules condensed on the gold surface. The spectrometer covers 700–4000 cm^{-1} with a typical resolution of 1 cm^{-1} and an averaged spectrum consists of a total of 256 scans. Ice evaporation is induced by linear heating of the substrate (and ice) in TPD experiments. RAIR spectra are acquired simultaneously to monitor the ice composition during the TPD. A quadrupole mass spectrometer (QMS) is positioned at 4 cm, facing the ice sample to continuously analyze the gas-phase composition mass-selectively and to obtain desorption curves of evaporating molecules during the TPD experiments.

Mixtures and pure gas samples are prepared from $^{13}CO_2$ (Indugas, min 99% of ^{13}C), CO_2 (Praxair, 99% purity), ^{13}CO (Cambridge Isotope Laboratories, 98% purity) and from gaseous water at the saturation pressure of a de-ionized liquid sample at room temperature. The de-ionized water is purified by three freeze-pump-thaw cycles. The samples are prepared separately, then injected in the chamber via an inlet pipe directed along the normal of the gold surface. In all gas samples, an isotopologue of CO was used to separate the QMS signal from background CO and N_2. Similarly, an isotopologue of CO_2 was used to minimize the overlap in RAIR spectra between CO_2 ice and atmospheric CO_2 gas outside the UHV chamber.

H_2O and CO_2 ice amounts are determined directly using the RAIRS band strengths provided by Öberg et al. (2009c,a) for CRYOPAD. From these measurements the absolute ice thicknesses are known within 50%. The relative ice abundance uncertainties are smaller, ~20%, and due to small band strength variations with ice composition and temperature.

Table 1 lists the set of TPD experiments performed to calibrate and test the desorption model presented in Sect. 2.1. The TPD experiments begin with the deposition of pure or mixed ice samples on the gold substrate cooled to 16–19 K, and continue with a slow heating of the ices at a constant specified rate until the desorption of the molecules from the surface is complete. The evaporated gas phase molecules are continuously monitored by the QMS. RAIR spectra of the ices are acquired before heating to determine ice thicknesses and mixture ratios as described above. Spectra are also recorded during the warm-up as a second independent way to determine the ice composition and to monitor eventual structure modifications.

The infrared data are reduced by subtracting a local baseline around the molecular features. Mass spectrometric data are reduced by subtracting the ion current from species present in the background for each mass channel. Absolute yields cannot be directly obtained by the QMS since it is situated away from the ice sample (4 cm) and thus some of the desorbing molecules may get pumped away before detection. All QMS desorption rate curves are therefore normalized in such a way that the time-integrated desorption rate from the various species corresponds to their infrared spectrally measured ice abundance at the beginning of each experiment.

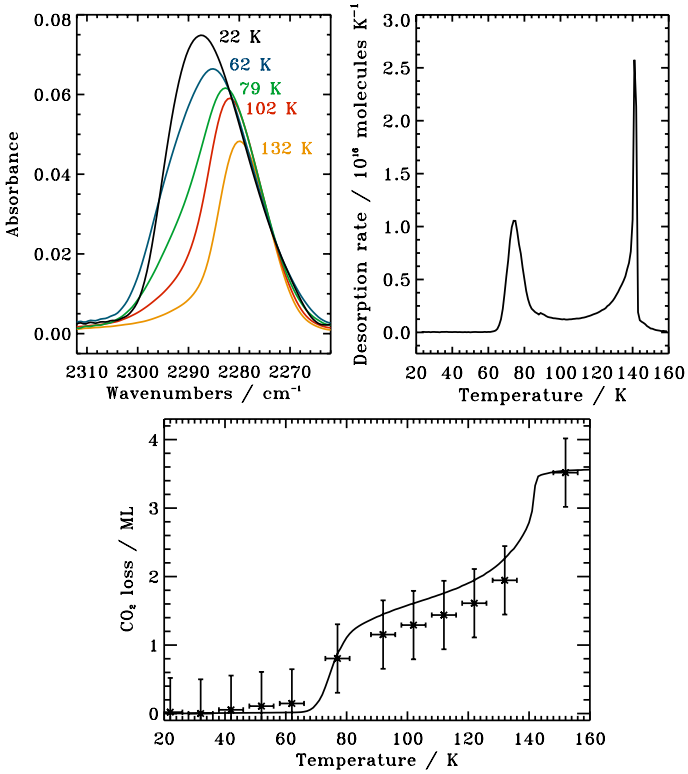

Fig. 2. The *upper left panel* presents the infrared CO_2 stretching features at specific temperatures during the warm-up of 18 ML of a H_2O:CO_2 5:1 ice heated at 1 K.min^{-1}. The *right upper panel* presents the desorption rate of CO_2 for the same experiment obtained by mass spectrometry. The bottom panel shows the ice loss for this experiment obtained by infrared measurements (crosses) and mass spectrometry (solid line).

4. Experimental analysis

4.1. Complementarity of RAIRS and QMS

Figure 2 illustrates the agreement between desorption curves derived from QMS and RAIRS data for CO_2 in a 5:1 water-dominated H_2O:CO_2 ice, 18 ML thick and heated at 1 K.min^{-1} rate (Exp. 11). The upper left panel in Fig. 2 shows the CO_2 stretching band recorded at different temperatures during warm-up: after ice deposition at 22 K, at 62 K where segregation is known to be efficient (Öberg et al. 2009b), during the first ice desorption peak around 79 K, in the temperature interval between pure CO_2 desorption and H_2O desorption, and during desorption of the trapped CO_2. The right panel shows the desorption rate of CO_2 derived from the same experiment by mass spectrometry. The bottom panel presents the cumulative ice loss versus temperature for this experiment, obtained both by integrating the CO_2 mass signal with respect to the temperature, and by integrating the CO_2 infrared signal recorded at specific temperatures. The error bars on the infrared data are due to variable ice band strengths with temperature and composition. Within these uncertainties the fractional ice loss curves derived by infrared and by mass spectrometry agree well; there seems to be only a small systematic offset for the 80–130 K range. This implies that the first RAIR spectrum of the ice after deposition can be used to derive quantitative results from the TPD experiments.

Figure 2 also shows that there is evidence for some ice loss between the two main desorption peaks. The cumulative QMS and infrared spectroscopy signals match each other at these intermediate temperatures, which points to that the measurements trace actual ice desorption in between the pure ice desorption event and the desorption of trapped volatiles. The implications of this ice desorption process is discussed below, but it is important to note that this is not incorporated into the model framework and this may be a limitation to step-wise desorption models, whether using our parameterization or any of the previously published ones. Quantifying this process would require an additional set of experiments where the mass spectrometer is mounted closer to the substrate to allow for the detection of very low desorption rates.

4.2. Desorption trends

Figure 3 shows the desorption of CO_2 from H_2O:CO_2 ice mixtures of different thicknesses (a), with different CO_2 concentrations (b), and heated at different rates (d). In addition there are two CO TPD curves from H_2O:CO mixtures with different CO concentrations (c). For reference, Fig. 3e) presents the TPD curves of pure CO, CO_2, and H_2O ice heated at 1 K min^{-1}. The fraction of trapped volatile is obtained by integrating the QMS signal for temperatures above 110 K and dividing it by the QMS signal integrated over the entire 20–160 K range. The chosen temperature of 110 K is well below the onset of the second desorption peak and the volatiles that desorbed during the first CO_2 or CO desorption peak are (almost) entirely pumped, though as discussed above there seems to be a low-level type of desorption occurring between the main desorption peaks. Whether due to finite pumping or actual desorption this results in a 10–20% uncertainty in the determination of the trapped fraction, i.e., the choice of temperature integration limits affects the estimated amount of trapped ice by <20%. The trapped percentage of volatiles in each experiment, defined with respect to the initial volatile ice content, is reported in the second last column of Table 1. The last column of Table 1 presents the trapped abundance of volatiles

Table 1. Overview of the desorption experiments.

Exp.	Sample	Ratio	Thick. (ML)	Heat. rate (K.min^{-1})	Trapped CO_2/CO ice % wrt. CO_2/CO	wrt. H_2O
1	H_2O	–	24	1	–	–
2	$^{13}CO_2$	–	6	1	–	–
3	^{13}CO	–	6	1	–	–
4	H_2O:CO_2	10:1	12	1	62	6.2
5	H_2O:CO_2	10:1	19	1	75	7.5
6	H_2O:CO_2	10:1	32	1	84	8.4
7	H_2O:$^{13}CO_2$	5:1	32	1	64	12.8
8	H_2O:$^{13}CO_2$	5:1	18	10	62	12.4
9	H_2O:$^{13}CO_2$	5:1	18	1	53	10.6
10	H_2O:$^{13}CO_2$	5:1	10	5	44	8.8
11	H_2O:$^{13}CO_2$	5:1	10	1	45	9.0
12	H_2O:$^{13}CO_2$	5:1	10	0.5	44	8.8
13	H_2O:^{13}CO	10:1	14	1	43	4.3
14	H_2O:^{13}CO	10:1	25	1	47	4.7
15	H_2O:^{13}CO	5:1	20	1	24	4.8
16	H_2O:^{13}CO	2:1	13	1	9	4.5
17	H_2O:^{13}CO	1:1	17	1	4	4.0
18	H_2O:CO_2:^{13}CO	11:4:1	16	1	32/19	12/2
19	H_2O:CO_2:^{13}CO	20:1:1	30	1	92/96	5/5

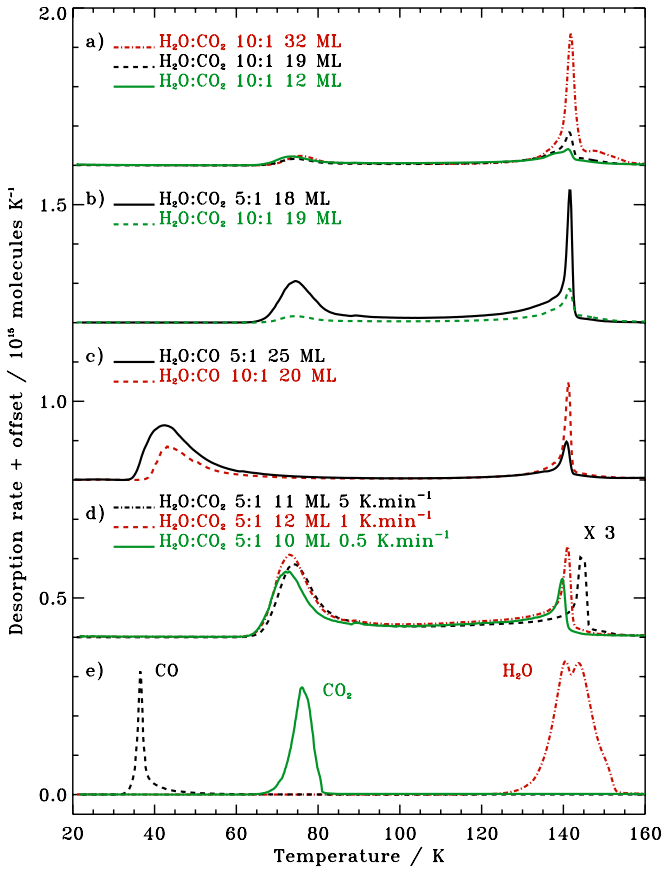

Fig. 3. Experimental CO and CO_2 desorption curves **a)**–**d)** during warm up of ice mixtures (offset for visibility) together with pure CO, CO_2 and H_2O ice TPD curves **e)**. The heating rate is 1 K.min^{-1} except for when specified otherwise in **a)**, the total ice thickness and mixing ratio are listed in for each experiment.

species with respect to the initial H_2O abundance. This value is less variable compared to the trapped amount of CO/CO_2 with respect to the initial CO/CO_2 abundance presented in the preceding column. Both Table 1 and Fig. 3 show that for CO_2 and CO the percentage of trapped volatile species in the H_2O ice is highly dependent on the experimental conditions; the CO_2 trapping fraction varies between 44 and 84% with respect to the initial volatile content. In the following subsections, we report and discuss these dependencies.

4.2.1. Thickness dependency

Figure 3a presents the desorption of a H_2O:CO_2 10:1 ice mixture for different initial ice thicknesses and shows that the amount of trapped CO_2 (desorption around 140 K) increases with ice thickness. In contrast the amount of CO_2 desorbing around 70 K is independent of ice thickness in the experimentally investigated range. This implies that only CO_2 molecules from the top part of the ice are available for desorption at the CO_2 desorption temperature. This can be explained by either a highly porous ice that allows CO_2 to "freely" desorb from the top layers or by diffusion from the top layers of the mantle phase to the surface. In both cases the surface is eventually totally saturated by water molecules, trapping the rest of the volatiles in the ice mantle.

4.2.2. Mixing ratio dependency

The dependence of the volatile trapping with the mixture ratio is presented in Fig. 3b) for H_2O:CO_2 and in Fig. 3c) for H_2O:CO ice mixtures. In both cases the trapped fraction decreases as the volatile to H_2O ratio increases. In other words, the amount of pores exposed to the surface or the diffusion length scale of volatiles in the ice must increase with increasing volatile concentration. A similar dependency was noted in Öberg et al. (2009b) when measuring segregation in ices. Increased diffusion may either be due to a gradually looser binding environment in the volatile-rich ices or a break-down of H_2O ice structure in the presence of higher concentrations of volatiles. The thick H_2O:CO ice experiments (Exps. 14, 15 and 17) with initial mixture ratios of 10:1, 5:1 and 1:1 show a continuous decline of the trapping fraction, which suggests that either the ice becomes continuously more porous or that the diffusion path length increases gradually with volatile concentration.

4.2.3. Molecular dependency

Similarly to Sandford & Allamandola (1990) and Collings et al. (2004) we find that the trapping efficiencies of the investigated CO_2 and CO in H_2O ice are radically different. When comparing Figs. 3b) and c), it appears that CO is much more mobile than CO_2 in the H_2O ice as demonstrated by the higher trapping fraction of CO_2 compared to CO in similar H_2O ice mixtures. Sandford & Allamandola (1990) explained this difference from a combination of different binding energies of CO and CO_2 in H_2O ice due to molecular size, shape and electronic differences. These binding energies may equally affect the probability of escaping through an ice pore or diffusing through the bulk of the ice.

4.2.4. Heating rate dependency

In Fig. 3d, the heating rate of the ice is varied for a H_2O:CO_2 5:1 ice of 10−12 ML between 0.5, 1 and 5 K.min^{-1}. This does not appreciably affect the trapping efficiency of CO_2 in the H_2O ice and implies that the process responsible for exchanges between the surface and the mantle is fast compared to the experimental warm-up time. If this was not the case, a lower heating rate would have resulted in a smaller amount of trapped CO_2, since a slower heating means more time for the migration of mantle molecules to the surface.

The lack of a heating rate dependency on the trapped amount of volatiles (same trapped percentage in Exp. 10, 11 and 12) also implies that there is a rather sharp boundary between the molecules in the upper layers that can diffuse to the surface (whether through pores or bulk diffusion) and molecules deeper in the ice that cannot. Even if the volatiles deep in the ice can diffuse within the ice mantle, diffusion "upwards" must quickly become slow as the surface layers saturate with H_2O molecules or alternatively all accessible pores have been emptied. This explains that the amount of desorbing CO_2 molecules at low temperatures is thickness independent (the H_2O "ice cap" will become impenetrable after a certain amount of CO_2 molecules have desorbed) and that entrapment efficiencies are unaffected by lower heating rates.

4.3. Tertiary mixtures

The desorption rates for the tertiary mixtures (Exps. 18 and 19) are presented in Fig. 4a). Similarly to the binary experiments, the trapping of volatiles is more efficient for a lower volatile to H_2O ratio. The desorption curves for CO_2 are not affected by the presence of CO. Thus the CO-CO_2 interaction does not have a significant impact on the amount of CO_2 trapped within the water matrix. Overall the TPD curves resemble the addition of desorption curves from two separate binary mixtures, except for a small fraction of CO that desorbs with CO_2 in the H_2O:CO_2:CO 11:4:1 mixture (lower panel in Fig. 4). It is unclear whether this desorption is due to a co-desorption of CO with CO_2 or to a release of CO that has been trapped under a barrier of CO_2 surface molecules. The observed similarity supports the use of binary ice mixtures as templates to study diffusion and desorption even though they are not directly representative of interstellar ice mixtures.

When comparing the desorption of CO from a tertiary and a binary ice mixture with the same H_2O:CO ratio and ice thickness, it appears that less CO is trapped in the tertiary mixture. This may be due to ice structure changes, as discussed above, or to shielding of CO from the sticky water molecules by CO_2

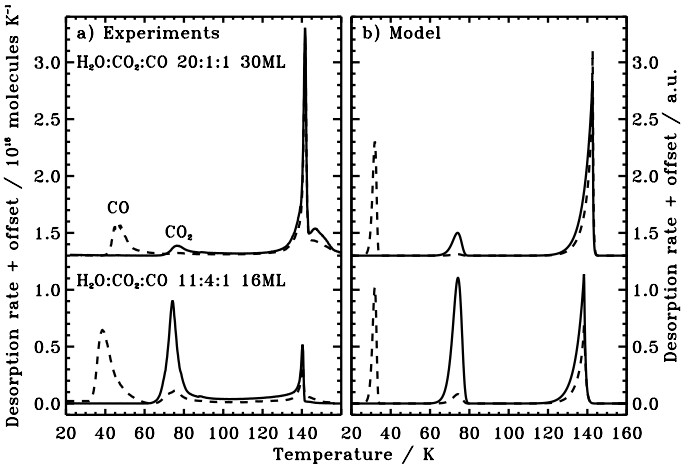

Fig. 4. a) Desorption rate of CO_2 (solid line) and CO (dashed line) from two tertiary water dominated ice mixtures (Exps. 18 and 19) with a 1 K.min^{-1} heating rate. – **b)** Implemented three-phase model desorption rate for the same eperiments.

molecules (the CO-CO_2 bond is weaker than the H_2O-CO one), lowering the CO diffusion barrier. The CO_2 and CO desorption curves from the dilute tertiary mixture both contain a small additional peak around 150 K, only seen elsewhere in the thickest H_2O:CO_2 10:1 ice experiment. A similar double peak was noted in the 20:1 desorption experiments of Collings et al. (2004).

4.4. Ice diffusion mechanisms: pore versus bulk diffusion

The main mechanism behind diffusion in the ice mantle is not known and may differ between different ices. Most previous studies have focused on diffusion in cracks and pores and pore collapse has been introduced to explain ice trapping. The observation that both CO and CO_2 become trapped even though they partly desorb at their, very different, pure ice desorption temperatures is difficult to reconcile with pore collapse as the main trapping mechanism, however. That is, it would imply efficient H_2O pore collapse both at ∼30 K and ∼70 K.

Even if pore collapse does not provide a complete explanation of why ices become trapped, some kind of internal surface hopping may explain why molecules can diffuse out of the ice. In this scenario, the CO_2 desorption ice thickness dependency is due to that the pores and cracks that are open to the surface only go down to a certain depth, in this case a few ML for H_2O:CO_2 5:1. The different CO and CO_2 trapping efficiencies may then be either due to different ice structures or to CO desorbing easier through pores compared to CO_2. Pore diffusion may thus be consistent with these particular experimental results, but ice diffusion is present also in other ices that are known to be quite compact, e.g. CO ice (Bisschop et al. 2006). While it is possible that diffusion occurs through completely different mechanisms in different ices, the concept of ice bulk diffusion has the prospect of approximating mixing and de-mixing processes in all kinds of ices, regardless of structure.

In the bulk diffusion scenario, an amorphous ice is viewed like a very viscous liquid, whose viscosity decreases with the volatility of the ice molecules. In Öberg et al. (2009b) this was modeled as molecules swapping places with a barrier significantly higher than surface hopping. Volatile molecules will tend to swap their way towards the surface because it is energetically favorable to have the molecules that form weaker bonds in the

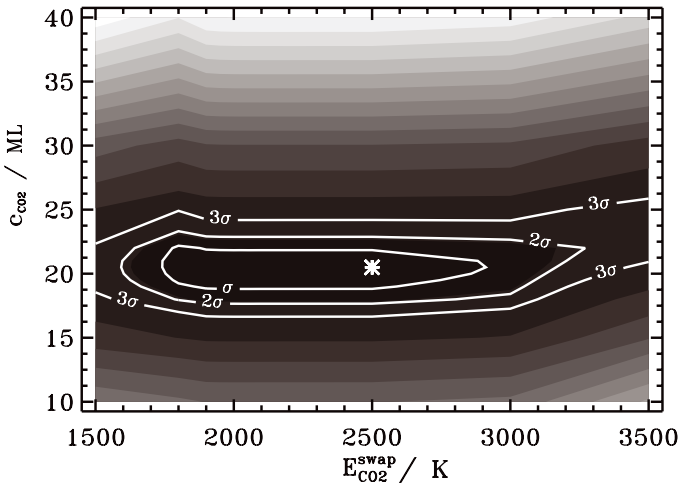

Fig. 5. χ^2 contour plot for fitting the model parameters $\epsilon^{swap}_{H_2O-CO_2}$ (parameterizing the ability of CO_2 to switch position with a H_2O molecule) and c_{CO_2} (parameterizing the CO_2 ice thickness where swapping is fast compared to the investigated heating rates) using the experimentally determined amount of CO_2 trapped in a binary H_2O:CO_2 ice (Exps. 4 to 12). These two parameters regulate the distribution of the volatile molecules in the gas, surface and mantle according to Eqs. (11) and (10) of Sect. 2.1.

surface layer (where fewer bonds can be made due to the ice-vacuum interface). Trapping is explained by that when volatile molecules diffuse from the top mantle layers to the surface and desorb, the top mantle layers become saturated with H_2O and therefore viscous enough to be impenetrable. The low desoption rate of volatiles between the volatile and H_2O ice desorption peaks would however suggest that under some experimental conditions, small amounts of volatiles can escape through this H_2O barrier. More experiments are required to test under which conditions this is a reasonable approximation. The model presented below is an attempt to include the most important features of this concept while still keeping the number of parameters low.

5. Model parametrization and performance

5.1. Parametrization

The pure ice desorption energies are derived from fitting the three-phase model to the experimental pure ice desorption curves with the results: E_{H_2O} = 4400 K, E_{CO_2} = 2440 K and E_{CO} = 1010 K. The H_2O value is lower than the one found in Fraser et al. (2001). This discrepancy is probably due to a combination of that we use a single experiment, do not include the pumping speed and fix the pre-exponential factor to $\nu = 10^{12}$ s^{-1} for every species here. The value in Fraser et al. (2001) should thus still be used when modeling the absolute desorption temperature. For the purpose of parameterizing the desorption fractions we prefer our value for the sake of consistency. The remaining model parameters $\epsilon^{swap}_{H_2O-i}$ and c_i are obtained separately for CO_2 and CO. This is done through a χ^2 analysis, where trapping fractions from the model are compared to those from the binary experiments for a grid of $\epsilon^{swap}_{H_2O-i}$ and c_i values. The minimum χ^2 value for CO_2 is obtained for $\epsilon^{swap}_{CO_2-H_2O}$ = 2500 K, c_{CO_2} = 20.5 ML, but the swapping energy for H_2O:CO_2, which is linked to the ability of CO_2 to swap with H_2O within the solid phase, is not well-constrained between 1600–3200 K (Fig. 5). In contrast, the parameter c_{CO_2} related to available amount of CO_2 from the ice mantle that can migrate to the surface, is well constrained which suggests that even at laboratory time scales mixture desorption is mainly governed by how large a part of the mantle is eligible for swapping with the surface, rather than the swapping barriers.

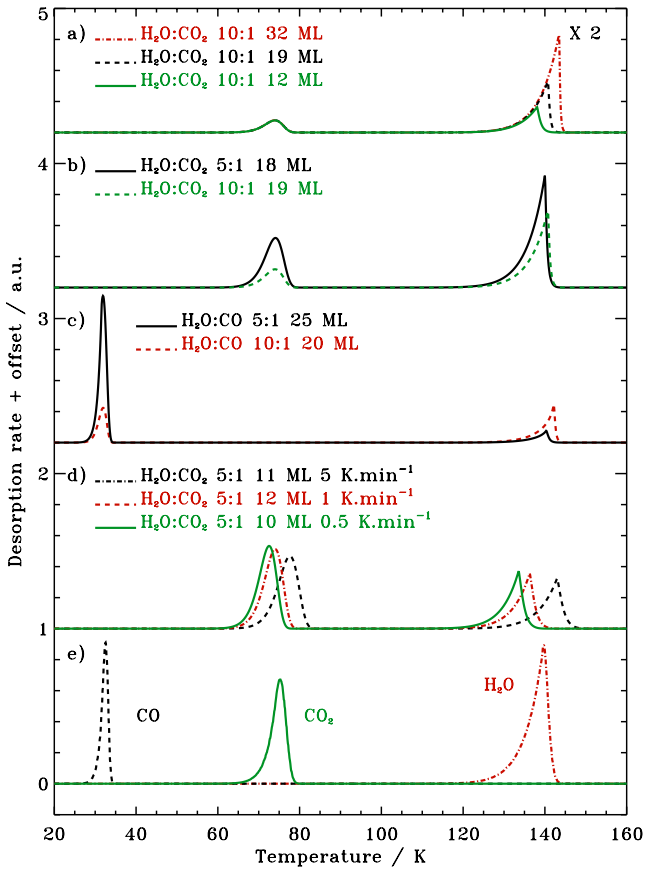

Fig. 6. Simulated CO_2 and CO TPD curves from H_2O:CO_2 and H_2O:CO mixtures for different thicknesses, ratios, and heating rates **a)**–**d)**. Panel e) presents the simulated desorption of pure H_2O, CO_2 and CO ice. This figure connects the model outputs to the experiments shown in Fig. 3.

The CO experiments can be fitted with $\epsilon^{swap}_{CO-H_2O}$ = 960 K and c_{CO} = 80 ML, but these are based on only a few experiments and the inequalities $\epsilon^{swap}_{H_2O-CO} \langle \epsilon^{swap}_{H_2O-CO_2}$ and $c_{CO} \rangle c_{CO_2}$ are alone well constrained.

5.2. Model performance

5.2.1. Desorption trends modeling

Figure 6 shows the simulations of the binary mixture desorption using the optimized model parameters from the previous section. Generally the qualitative agreement is good and the model captures the trends that were observed experimentally. The exact shapes of the modeled and experimental desorption curves differ for several reasons. First, the model does not take into account the range of environments from which the molecules desorb, e.g., the H_2O/volatile fraction changes during the desorption process and even a pure ice has a range of different binding sites. This affects both the position and the width of the peak. Second, the model does not consider the different water ice structures present at different temperatures; water ice crystallizes around 140 K (see the desorption peaks for water in Fig. 3e), which may affect the shape and position of the second desorption peak of the volatiles. Finally, the model does not include finite

pumping speeds, which results in abundance tails in the experimental curves. While these effects may all be important under special circumstances the aim of the extended three-phase model is not to reproduce the experimental results perfectly. Rather, the goal is to capture the main characteristics of ice mixture desorption.

The increase of the trapped amount of volatiles with ice thickness and the experimental observation that the same amount of molecules desorbs around the volatile pure desorption temperature, regardless of the ice thickness, are reproduced in the model because diffusion between the mantle and surface is only allowed from a fraction of the mantle, f_i (Eq. (11) in Sect. 2.1) which depends on the kind of volatile and mixing ratio with water. This fraction is independent of the ice thickness. Thus the same amount of volatile molecules migrates to the surface regardless of ice thickness, followed by saturation of the surface phase by water molecules. The rest of the volatiles is trapped in the mantle until H_2O desorption, thus the trapped fraction depends on the ice thickness.

The observed concentration effect on the trapping efficiency is reproduced by the model because the fraction of volatiles migrating to the surface depends on the mixing ratio of the volatile with respect to water, $x_i^{\rm ini}$. The lower the concentration of volatiles in the ice is, the smaller the fraction of volatile molecules make it to the surface and the more become trapped. The higher mobility of CO compared to CO_2 is also reproduced by the model as the molecular paramater c_{CO_2} is lower than c_{CO}. Thus more volatiles are able to diffuse to the surface in the case of H_2O:CO mixtures.

Experimentally, a low desorption rate is sometimes observed between the volatile and H_2O desorption temperature. In the model, the diffusion barrier energy is low enough that the diffusion process is complete before desorption of the volatile takes place and therefore there is no desorption between the pure and H_2O desorption peaks. Such a low diffusion energy barrier is needed to reproduce that the trapping efficiency is insensitive to the heating rate (within the explored heating rate range). There is probably a second diffusion process at play at these intermediate temperatures, which cannot be reproduced by the current, simple parameterization.

5.2.2. Quantitative agreement

Figure 7 compares the volatile trapping fractions obtained by the optimized H_2O:CO_2 model to those found experimentally. The error bars include the uncertainties due to the choice of the temperature from which we integrate the second QMS peak and are between 10–20% for the different experimental data points. The error bars on the model results originate from the uncertainties in the input ice thicknesses, mixing ratios and binding energies and these were obtained by varying the model input values within the experimental uncertainty ranges and then comparing the model results. In general, the uncertainty in the mixing ratio has the largest effect, resulting in model prediction uncertainties of ~15%. We conclude that CO_2 desorption from binary mixtures is quantitatively described by the model.

5.2.3. Predictive power

Figure 4b shows the output of the model for the H_2O:CO_2:CO tertiary ice mixture experiments (Exp. 18 and 19). These experiments were not used to constrain the model and are as a test of its predictive power. The concentration dependency in these experiments is reproduced by the model; an increase in the concentration of volatiles leads to a decrease in the trapping fraction.

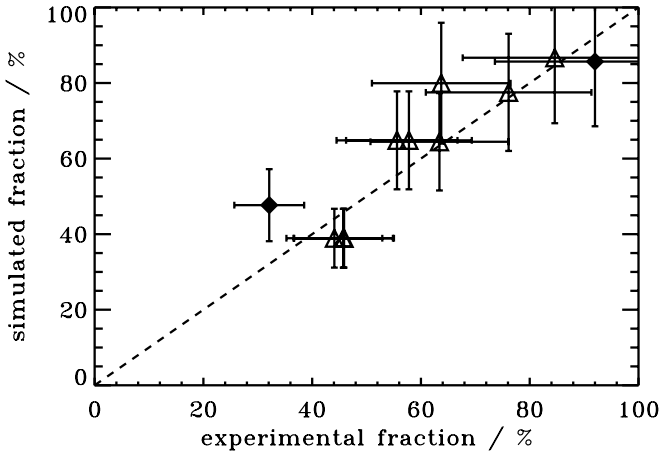

Fig. 7. Percentage of CO_2 experimentally trapped vs the simulated one. The triangles are the trapped percentages obtained from the binary mixture experiments. The diamonds are the model predictions for the two tertiary mixtures. The one-to-one ideal relation is plotted as a dashed line.

For the higher concentration mixture, H_2O:CO_2:CO = 11:4:1 (Fig. 4b, bottom panel), the model gives a CO desorption peak around 70 K (corresponding to the pure CO_2 desorption temperature), peak that was also experimentally observed (Fig. 4a, bottom panel). In the model, this peak results from the formation of free desorption sites on the surface due to desorption of surface CO_2. CO molecules that are mixed with water migrate to and desorb from the surface easily since the swapping and binding energies are very low compared to the CO_2 values.

In addition to reproducing these qualitative trends for tertiary mixtures, the three-phase model also treats correctly the desorption order of both CO_2 desorption peaks. Finally Fig. 7 shows that the model provides a reasonable quantitative agreement between the predicted and experimentally determined amounts of CO_2 trapped in the tertiary ice mixtures (black diamonds). This is very promising for extending this proof-of-concept model to more species and more complex mixtures.

6. Astrophysical implications

Trapping of volatiles in H_2O ice is a crucial parameter when predicting the chemical evolution during star and planet formation (Viti et al. 2004). The modified three-phase desorption model is used here to test the effect of different initial ice compositions and ice thicknesses on ice mixture desorption. Ultimately the three-phase model should, however, be integrated in a protostellar collapse model to simulate the ice desorption accurately during star formation. The prime advantage of the three-phase model, as initially introduced by Hasegawa & Herbst (1993) and extended here, is that it can treat surface and ice chemistry correctly, since it differentiates between surface molecules that can react with gas phase molecules, and mantle molecules that are protected from further processing.

Figure 8 shows the amount of CO_2 ice with respect to the original H_2O ice abundance as a function of temperature for different ice thicknesses and mixing ratios heated at 1 K per 100 years, typical for infall of material during protostar formation (Jørgensen et al. 2005).

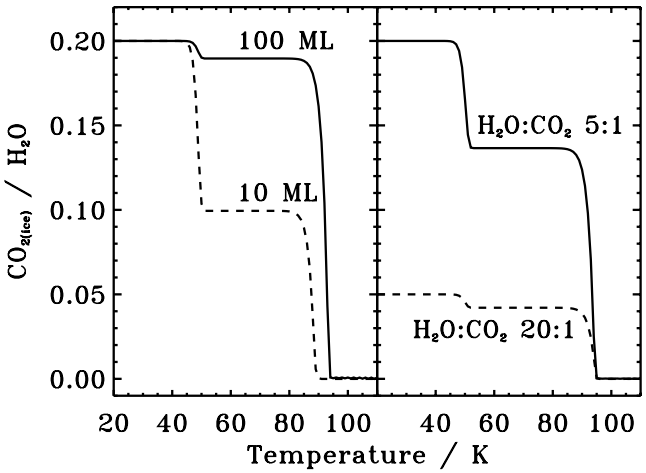

Fig. 8. The amount of CO_2 ice during ice warm-up at 1 K per 100 years according to the three-phase model, assuming two different initial H_2O:CO_2 5:1 ice mixture thicknesses (*left panel*) and two different 20 ML ice mixing ratios (*right pannel*).

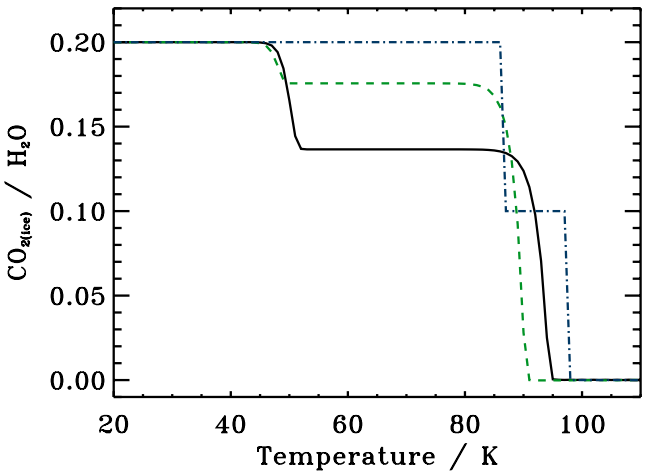

Fig. 9. Amount of CO_2 ice during ice warm-up for a H_2O:CO_2 5:1 ice 20 ML thick simulated by different models: the implemented three-phase model described here (black solid line), the original three-phase model by Hasegawa & Herbst (1993) (green dashed line), the Viti et al. (2004) model (blue dash-dotted line). A heating rate of 1 K per century is used in the two first models and desorption around a 5 solar masses protostar is presented from the Viti et al. (2004) model case.

The percentage of CO_2 entrapment in a diluted water ice is significantly affected by the initial ice thickness and mixing ratio; 50% of the initial CO_2 abundance is trapped in a 10 ML ice and 95% in a 100 ML ice. A similarly dramatic difference is seen when assuming different initial ice mixtures: 64% of the CO_2 stays trapped in the 5:1 ice and the fraction increases to 84% for the 20:1 ice.

The treatment of these trapping dependencies is one of the key strengths of the extended three-phase desorption model presented here. Figure 9 compares CO_2 ice desorption from a H_2O:CO_2 ice using the extended three-phase model, the original three-phase model by Hasegawa & Herbst (1993), and the Viti et al. (2004) astrochemical network. Assuming a 20 ML thick H_2O:CO_2 5:1 ice heated at 1 K per century, our model predicts that 64% of the initial CO_2 will be trapped by the water ice, while the model by Hasegawa & Herbst (1993) predicts an 80% trapping amount. This difference originates from the lack of mantle-surface diffusion in Hasegawa & Herbst (1993). Its implementation is clearly important to correctly treat trapping of volatiles and to account for segregation observed around protostars (Ehrenfreund et al. 1998; Pontoppidan et al. 2008).

All the CO_2 molecules are predicted to be trapped by the water ice when simulating H_2O:CO_2 ice desorption with the Viti et al. (2004) model. The Viti et al. (2004) model assumes a different heating rate compared to the one used for the two three-phase models, but this only affects the desorption temperatures and does not affect the volatiles trapping fractions. Instead, the high trapping fraction is due to the fact that the model was parametrized based on a desorption experiment performed for a H_2O:CO_2 ice with a ratio of 20:1, which differs from the 5:1–4:1 ratio found in dense molecular clouds and protostellar envelopes (Knez et al. 2005; Pontoppidan et al. 2008). In the case of a H_2O:CO_2 20:1 ices, our model outputs agree well with 100% trapping fraction used by Viti et al. (2004), since we find that more than 95% of the CO_2 is trapped by the water ice for 10–100 ML thick ices.

These different model predictions demonstrate the need for systematic laboratory studies when modelling ice desorption, since ice properties, such as ice thickness and mixing ratio, affect the desorption process. Even when using desorption step functions, the size of the step cannot be accurately decided from a single experiment. Rather the investment of multiple experiments are needed, together with their efficient parameterization, to obtain versatile models of ice desorption for arbitrary initial conditions. Already for binary ice mixtures, this results in large experimental data sets. It is therefore reassuring that using binary mixtures as templates for more complex ice mixtures results in approximately the correct trapping predictions.

7. Conclusions

Desorption from H_2O-rich ice mixtures is complex in that the amount of trapped ice depends not only on the species involved, but also on the mixture ratio and the ice thickness; there is no constant fraction of volatile species trapped in a H_2O ice. This complex behavior can be reproduced by extending the three-phase model introduced by Hasegawa & Herbst (1993).

Using the H_2O:CO_2 ice system as a case study, we showed that a three-phase model that includes mantle-surface diffusion can reproduce the amount of trapped ice quantitatively in a range of binary ice mixtures. The appropriate input parameters for the H_2O:CO_2 system are a swapping energy $\epsilon^{\rm swap}_{\rm H_2O-CO_2}$ = 2250 K and a molecular parameter $c_{\rm CO_2}$ = 20.5 ML, which describes from which ice depth diffusion to the surface can occur.

In the model, the different CO_2 and CO behavior can only be reproduced if $\epsilon^{\rm swap}_{\rm H_2O-CO} < \epsilon^{\rm swap}_{\rm H_2O-CO_2}$ and $c_{\rm CO} > c_{\rm CO_2}$. This suggests that diffusion/molecule swapping in H_2O-rich ices depends equally on the breaking of the H_2O-volatile bond (parametrized here by the swapping barrier height) and on the mass/volume of the diffusing volatile (parameterized here by the ice thickness that the molecule can diffuse through). The experimental trends found for H_2O:CO and H_2O:CO_2:CO ice mixture desorption are consistent with the H_2O:CO_2 trends, which suggests that the three-phase model is generally appropriate to model ice mixture desorption.

However the ice desorption process is implemented in astrochemical models, this study demonstrates that it is vital to understand how ice mixture desorption depends on the ice characteristics. The extended three-phase model naturally treats ice

desorption with the right kinetic order and reproduces volatile entrapment. Its use in astrochemical networks for grain-gas interactions should improve the predictions of gas-phase and grain-surface species abundances in astrophysical environments.

Acknowledgements. This work has greatly benefitted from discussions with Ewine van Dishoeck and comments from an anonymous referee. Funding is provided by NOVA, the Netherlands Research School for Astronomy. Support for K. I. Ö. is provided by NASA through Hubble Fellowship grant awarded by the Space Telescope Science Institute, which is operated by the Association of Universities for Research in Astronomy, Inc., for NASA, under contract NAS 5-26555.

References

Aikawa, Y., Wakelam, V., Garrod, R. T., & Herbst, E. 2008, ApJ, 674, 984
Biham, O., Furman, I., Pirronello, V., & Vidali, G. 2001, ApJ, 553, 595
Bisschop, S. E., Fraser, H. J., Öberg, K. I., van Dishoeck, E. F., & Schlemmer, S. 2006, A&A, 449, 1297
Brown, W. A., & Bolina, A. S. 2007, MNRAS, 374, 1006
Burke, D. J., & Brown, W. A. 2010, Phys. Chem. Chem. Phys., 12, 5947
Collings, M. P., Dever, J. W., Fraser, H. J., & McCoustra, M. R. S. 2003, Ap&SS, 285, 633
Collings, M. P., Anderson, M. A., Chen, R., et al. 2004, MNRAS, 354, 1133
Collings, M. P., Dever, J. W., McCoustra, M. R. S., & Fraser, H. J. 2005, Highlights Astron., 13, 491
Doty, S. D., Schöier, F. L., & van Dishoeck, E. F. 2004, A&A, 418, 1021
Ehrenfreund, P., Dartois, E., Demyk, K., & D'Hendecourt, L. 1998, A&A, 339, L17
Fraser, H. J., Collings, M. P., McCoustra, M. R. S., & Williams, D. A. 2001, MNRAS, 327, 1165
Fuchs, G. W., Acharyya, K., Bisschop, S. E., et al. 2006, Faraday Discuss., 133, 331
Hasegawa, T. I., & Herbst, E. 1993, MNRAS, 263, 589
Jørgensen, J. K., Schöier, F. L., & van Dishoeck, E. F. 2005, A&A, 435, 177
Kimmel, G. A., Stevenson, K. P., Dohnálek, Z., Smith, R. S., & Kay, B. D. 2001, J. Chem. Phys., 114, 5284
Knez, C., Boogert, A. C. A., Pontoppidan, K. M., et al. 2005, ApJ, 635, L145
Öberg, K. I., van Broekhuizen, F., Fraser, H. J., et al. 2005, ApJ, 621, L33
Öberg, K. I., Bottinelli, S., & van Dishoeck, E. F. 2009a, A&A, 494, L13
Öberg, K. I., Fayolle, E. C., Cuppen, H. M., van Dishoeck, E. F., & Linnartz, H. 2009b, A&A, 505, 183
Öberg, K. I., van Dishoeck, E. F., & Linnartz, H. 2009c, A&A, 496, 281
Pontoppidan, K. M., Fraser, H. J., Dartois, E., et al. 2003, A&A, 408, 981
Pontoppidan, K. M., Boogert, A. C. A., Fraser, H. J., et al. 2008, ApJ, 678, 1005
Sandford, S. A., & Allamandola, L. J. 1988, Icarus, 76, 201
Sandford, S. A., & Allamandola, L. J. 1990, Icarus, 87, 188
Stevenson, K. P., Kimmel, G. A., Dohnalek, Z., Smith, R. S., & Kay, B. D. 1999, Science, 283, 1505
Teolis, B., Loeffler, M., Raut, U., FamÂů, M., & Baragiola, R. 2007, Icarus, 190, 274
van Dishoeck, E. F. 2006, Proc. Nat. Acad. Sci. USA, 103, 12249
Visser, R., van Dishoeck, E. F., Doty, S. D., & Dullemond, C. P. 2009, A&A, 495, 881
Viti, S., Collings, M. P., Dever, J. W., McCoustra, M. R. S., & Williams, D. A. 2004, MNRAS, 354, 1141